© 2017. Published by The Company of Biologists Ltd | Development (2017) 144, 4114-4124 doi:10.1242/dev.156752

RESEARCH ARTICLE

The African Zika virus MR-766 is more virulent and causes more severe brain damage than current Asian lineage and dengue virus

Qiang Shao[1,*], Stephanie Herrlinger[2,*], Ya-Nan Zhu[2], Mei Yang[1], Forrest Goodfellow[3], Steven L. Stice[3], Xiao-Peng Qi[4], Melinda A. Brindley[5] and Jian-Fu Chen[1,‡]

ABSTRACT

The Zika virus (ZIKV) has two lineages, Asian and African, and their impact on developing brains has not been compared. Dengue virus (DENV) is a close family member of ZIKV and co-circulates with ZIKV. Here, we performed intracerebral inoculation of embryonic mouse brains with dengue virus 2 (DENV2), and found that DENV2 is sufficient to cause smaller brain size due to increased cell death in neural progenitor cells (NPCs) and neurons. Compared with the currently circulating Asian lineage of ZIKV (MEX1-44), DENV2 grows slower, causes less neuronal death and fails to cause postnatal animal death. Surprisingly, our side-by-side comparison uncovered that the African ZIKV isolate (MR-766) is more potent at causing brain damage and postnatal lethality than MEX1-44. In comparison with MEX1-44, MR-766 grows faster in NPCs and in the developing brain, and causes more pronounced cell death in NPCs and neurons, resulting in more severe neuronal loss. Together, these results reveal that DENV2 is sufficient to cause smaller brain sizes, and suggest that the ZIKV African lineage is more toxic and causes more potent brain damage than the Asian lineage.

KEY WORDS: African ZIKV (MR-766), Asian ZIKV, DENV2, Brain damage, Neuronal death

INTRODUCTION

Zika virus (ZIKV) is an emerging *Flaviviridae* family member of significant public health concern. ZIKV infection during pregnancy causes severe congenital birth defects including microcephaly, fetal growth restriction, stillbirth, ocular disorders and CNS injury, among others (Brasil et al., 2016; Marrs et al., 2016; Ventura et al., 2016). ZIKV has two major lineages: the Asian lineage and African lineage. The Asian lineage is currently circulating in North, Central and South America, and induces congenital brain disorders (Faria et al., 2016; Haddow et al., 2012; Hamel et al., 2016). Historically, there is no scientific documentation of ZIKV-associated birth defects in Africa, where the virus originated. It has been speculated that the African lineage of ZIKV evolved into a more virulent form as it traveled from Africa to South America. It is also possible that African countries have limited health programs and, as a result, did not document ZIKV-associated birth defects, or that infection with this lineage causes early embryonic lethality prior to virus detection (http://time.com/4219240/zika-africa-origins-microcephaly-vaccine/). Whereas these observations have raised the possibility that the historical African lineage is less virulent than the current Asian isolates associated with birth defects, experimental evidence supporting this hypothesis is lacking. Direct comparison of the impact of these lineages in the developing brain has not been performed.

Dengue virus (DENV) is a single positive-stranded RNA virus with four serotypes (DENV1-4). DENV and ZIKV belong to the same *Flaviviridae* family, and both viruses spread primarily through *Aedes* genus mosquitoes (Faria et al., 2016; Hamel et al., 2016). DENV is currently co-circulating with ZIKV in Brazil, the area most impacted by the recent ZIKV outbreak (Nunes et al., 2012, 2014). Co-circulation and co-infection with different *Flaviviridae* family members is becoming a common phenomenon (Dupont-Rouzeyrol et al., 2015; Paniz-Mondolfi et al., 2016). DENV and ZIKV co-infection has also been identified in pregnant women, although pathological outcomes remain unknown so far (Villamil-Gómez et al., 2016). Recent studies showed a complex immunogenic crosstalk between ZIKV and DENV (Barba-Spaeth et al., 2016; Dejnirattisai et al., 2016; Priyamvada et al., 2016; Stettler et al., 2016; Swanstrom et al., 2016). Antibodies against E protein domain I/II (EDI/II) of ZIKV potently enhanced DENV infection *in vitro*, and lethally enhanced DENV disease in mice (Stettler et al., 2016). These emerging data raise the concern of the potential detrimental effects of DENV on the developing brain. However, the consequence of DENV infection in the developing brain remains largely unknown.

To fill in these knowledge gaps, we have performed intracerebral inoculation of embryonic mouse brains. We found that DENV2 is sufficient to cause microcephaly through enhanced cell death in neural progenitor cells (NPCs) and neurons. To understand why DENV has not been linked with congenital brain disorders, we performed a side-by-side comparison. We found that DENV2 grows slower and causes minimal neuronal death, resulting in less severe microcephaly than the currently circulating ZIKV Asian lineage (MEX1-44). Importantly DENV2-infected pups exhibited no postnatal lethality. To directly compare ZIKV African strains and ZIKV Asian strains, we performed a side-by-side intracerebral inoculation of MEX1-44 (Asian lineage) and MR-766, a brain-adapted African lineage strain. Experimental results showed that MR-766 is more potent in causing brain damage and postnatal mortality than MEX1-44. Our mechanistic studies suggest that MR-766 grows faster and causes much more NPC and neuronal death than MEX1-44.

[1]Center for Craniofacial Molecular Biology, University of Southern California, Los Angeles, CA 90033, USA. [2]Department of Genetics, Department of Biochemistry & Molecular Biology, University of Georgia, Athens, GA 30602, USA. [3]Regenerative Bioscience Center, University of Georgia, Athens, GA 30602, USA. [4]Key Laboratory of Animal Models and Human Disease Mechanisms, Kunming Institute of Zoology, Chinese Academy of Sciences, Kunming, Yunnan 650223, China. [5]Department of Infectious Diseases, Department of Population Health and Center for Vaccines and Immunology, University of Georgia, Athens, GA 30602, USA.
*These authors contributed equally to this work

‡Author for correspondence (Jianfu@usc.edu)

Q.S., 0000-0001-5307-8264; S.H., 0000-0002-6049-0246; M.Y., 0000-0001-9988-8991; F.G., 0000-0002-3717-9433; S.L.S., 0000-0001-5710-5872; X.-P.Q., 0000-0002-7982-7486; M.A.B., 0000-0002-4929-8085; J.-F.C., 0000-0002-8869-5913

Received 3 July 2017; Accepted 2 October 2017

Development (2017) 144, 4114-4124 doi:10.1242/dev.156752

RESULTS

DENV2 is sufficient to cause smaller brain sizes by inducing cell death in NPCs and neurons

To examine the effects of dengue virus (DENV) infection in the developing brain, we injected ~1 µl 3.4×10^5 TCID50/ml DENV2 into the cerebral ventricles of embryonic day 14.5 (E14.5) mouse brains. DENV2, strain S16803 (GenBank GU289914), was isolated from a patient sample from Thailand in 1974 and passaged in C6/36 cells. The virus was passaged twice in Vero cells by the World Reference Center for Emerging Viruses and Arboviruses (WRCEVA) before mouse injections. Pups survived after DENV2 inoculation. At postnatal day 5 (P5), DENV2-infected pups were smaller and infected brain sizes were significantly reduced compared with controls (Fig. 1A-C). We dissected out different organs, including kidney, liver, lung and heart, and found that individual organ masses were also decreased (Fig. 1C). After inoculation of E14.5 brains, DENV2 starts to induce growth restriction and organ size reduction in P3 pups (Fig. S1). These results suggest that DENV2 infection of embryonic brains is sufficient to cause growth restriction, including smaller brain sizes in mice.

Using antibodies against a Flavivirus group antigen, we detected extensive DENV2 in the cerebral cortex (Fig. S2A). Massive neuronal death has been detected in the developing brain after ZIKV infection, so we considered whether the same could be true of DENV2 (Shao et al., 2016). To understand the causes of DENV2-induced microcephaly, we first examined neuronal survival. DENV2 infection caused a significant increase in caspase 3- and TUNEL-positive neurons in the cerebral cortex compared with controls (Fig. S3A-C). DENV2 was able to infect NPCs labeled by Sox2 or nestin in the developing mouse brain (Fig. S2B,C). ZIKV infection has been found to cause NPC apoptosis and cell cycle arrest, contributing to microcephaly in mice (Cugola et al., 2016; Li et al., 2016; Miner et al., 2016; Shao et al., 2016). Therefore, we examined NPCs in mice infected with DENV2 and found that this virus also resulted in NPC cell death (Fig. S3D,E). Interestingly, there were no significant changes in CldU labeling and cyclin D1 staining in the ventricular/subventricular zone (VZ/SVZ) of mouse cortex after DENV2 infection (Fig. S4). These results suggested that DENV2 infection did not interfere with NPC proliferation, which was further supported by p-H3 and Ki67 staining (Fig. S5) and cell cycle length analysis in our subsequent studies (Fig. 3D). Together, these results suggest that DENV2 infection induces cell death in NPCs and neurons in the developing brain, resulting in a smaller brain size.

Asian lineage ZIKV causes more severe microcephaly than DENV2

Severe brain malformations have not been linked with DENV, whereas currently circulating ZIKV Asian lineage strains have been established to cause microcephaly and additional fetal brain abnormalities in mice (Li et al., 2016; Shao et al., 2016). We reasoned that DENV2 and ZIKV have different effects on the developing brain. To test this hypothesis, we performed a side-by-side comparison using DENV2 and MEX1-44. We injected Vero cell supernatant (mock), ~1 µl 3.4×10^5 TCID50/ml DENV2 or MEX1-44 into the cerebral ventricles of E14.5 brains (Fig. 1D).

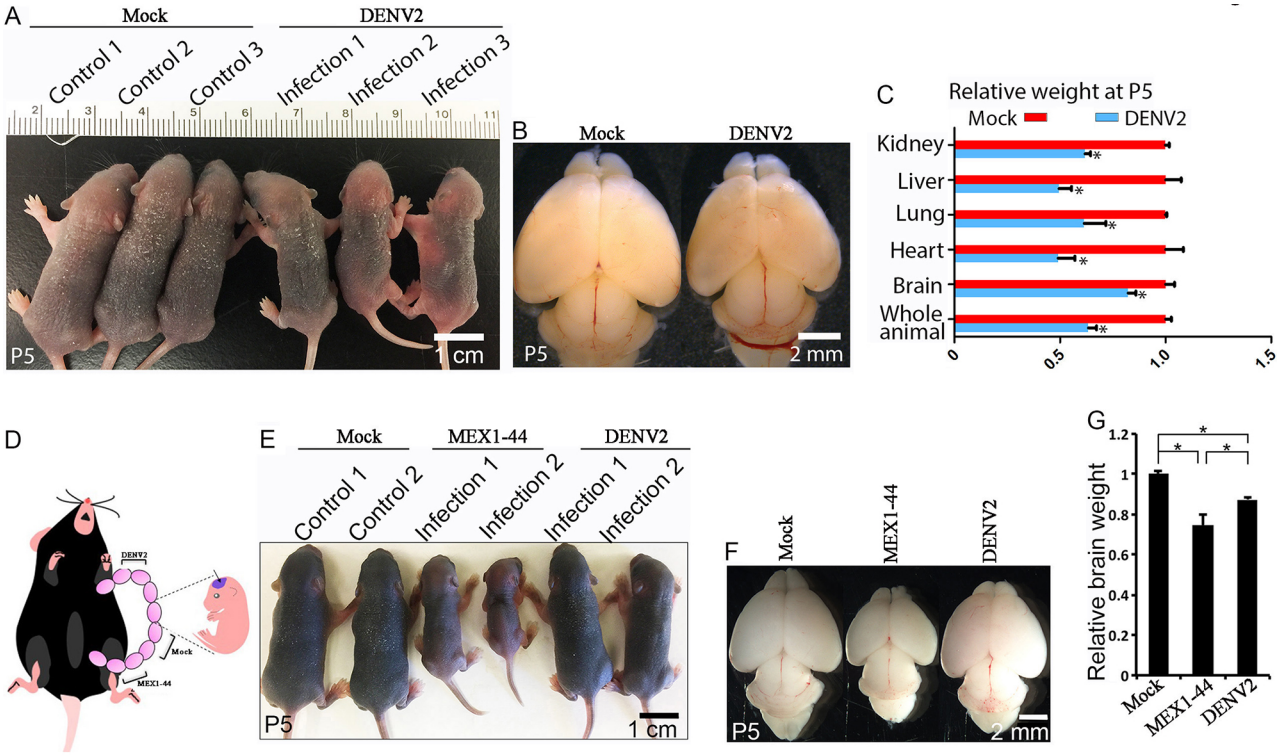

Fig. 1. DENV2 causes less severe microcephaly than MEX1-44. (A) Dorsal views of postnatal day 5 (P5) pups. ~1 µl 3.4×10^5 TCID50/ml DENV2 was injected into cerebral ventricles of embryonic day 14.5 (E14.5) brains followed by analyses at P5. Scale bar: 1 cm. (B) Dorsal views of P5 brains after DENV2 intracerebral inoculation of E14.5 mouse brains. Scale bar: 2 mm. (C) Relative weights of different organs from control or DENV2-infected pups at P5. Error bars indicate the s.e.m. of six independent experiments (*P<0.05, Student's t-test). (D) Experimental strategies of intracerebral inoculation of embryonic brains with mock, DENV2 or MEX1-44. (E) Dorsal views of postnatal day 5 (P5) pups. ~1 µl 3.4×10^5 TCID50/ml DENV2 or MEX1-44 were injected into E14.5 cerebral ventricles followed by analyses at P5. Scale bar: 1 cm. (F) Dorsal views of P5 brains. Scale bar: 2 mm. (G) P5 brain weights, relative to mock, from E14.5 intracerebral inoculation with vehicle (mock), DENV2 or MEX1-44. Error bars indicate the s.e.m. of six independent experiments. Two-way ANOVA analysis reveals a significant difference among different infections, *P<0.05.

Development (2017) 144, 4114-4124 doi:10.1242/dev.156752

MEX1-44 infection resulted in a drastic reduction in body size at P5 (Fig. 1E, middle), whereas DENV2 caused a relatively mild reduction in body size (Fig. 1E, right). Whereas DENV2-infected brains were slightly smaller and weighed less, MEX1-44 caused a substantial decrease in brain size and weight compared with controls (Fig. 1F,G). There was a significant difference in brain weight between DENV2- and MEX1-44-infected mice (Fig. 1G). Together, these results suggest that Asian lineage ZIKV causes more severe brain size reduction than DENV2 in the developing brain.

More neuron reduction and cortical thinning in Asian lineage ZIKV-infected brains compared with DENV2

To characterize virus-induced brain size reduction, we performed Hematoxylin and Eosin staining and found that the cortical radial thickness was significantly reduced in virally infected brains compared with mock-treated controls (Fig. 2A,B). MEX1-44 caused a more severe reduction in cortical thickness than DENV2 (Fig. 2A,B). Next, we quantified terminally differentiated neurons labeled by NeuN, a neuron-specific nuclear protein (Mullen et al., 1992). DENV2 infection led to a slightly decreased number of neurons, whereas MEX1-44 caused a much more severe reduction in the number of neurons compared with controls (Fig. 2C,D). Together, these results suggest that ZIKV causes more neuron loss in the developing brain, resulting in more profound cortical thinning and microcephaly compared with DENV2.

The cerebral cortex consists of a six-layer structure generated through the 'inside-out' mechanism of corticogenesis. Although earlier-born neurons reside in the deeper layers, later-born neurons migrate through existing layers to form the more superficial layers (Angevine and Sidman, 1961; Marín and Rubenstein, 2003). To determine whether cortical lamination is impaired and which layer(s) of neurons may be affected in virally infected brains, we

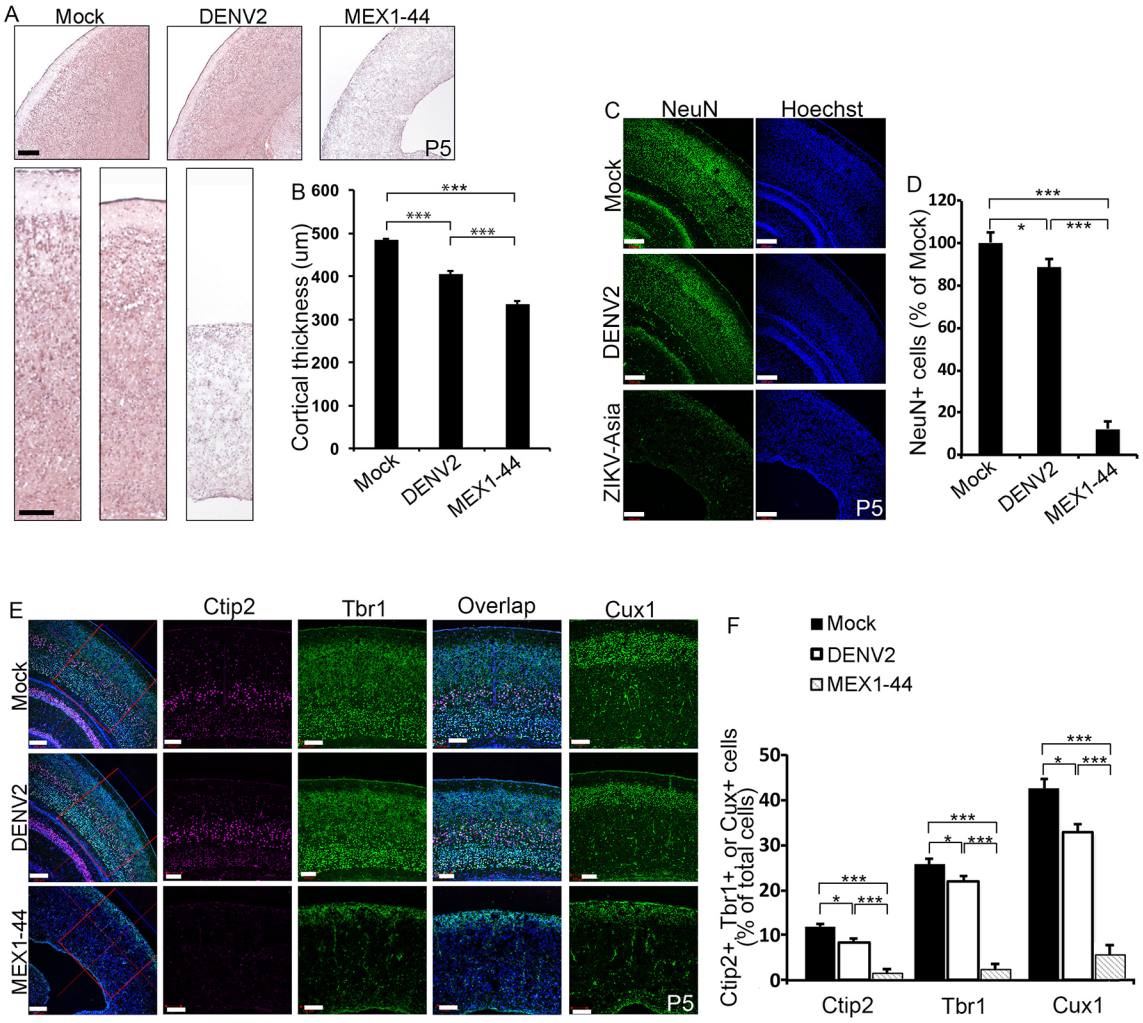

Fig. 2. MEX1-44 causes more neuron loss and cortical thinning than DENV2. (A) Coronal sections of P5 cerebral cortex stained with Hematoxylin and Eosin. Lower panels represent enlarged cerebral cortices from upper panels. Scale bars: 100 µm (upper panels); 50 µm (lower panels). (B) Quantification of cortical radial thickness from experiment in A. Error bars indicate s.e.m. of nine sections from three independent experiments. Two-way ANOVA revealed a significant difference among different infections, ***P<0.001. (C) Confocal imaging of P5 cerebral cortex stained with antibodies against NeuN (green). Hoechst stains nuclei (blue). Scale bars: 200 µm. (D) Quantification of the percentage of NeuN-positive cells out of total cells in virally infected cortexes normalized to mock-treated controls. Error bars indicate s.e.m. of nine sections from three independent experiments. Two-way ANOVA revealed a significant difference among different infections, *P<0.05 and ***P<0.001. (E) Confocal microscope images of coronal sections from P5 cortex stained with antibodies against Ctip2 (purple), Tbr1 (green) and Cux1 (green). Hoechst stains nuclei (blue). The four rightmost panels are enlargements of the regions outlined by red boxes in left panels. Scale bars: 200 µm (left panels); 100 µm (right panels). (F) Quantification of the percentage of Ctip2-, Tbr1- and Cux1-positive cells out of total cells in the boxed areas of P5 cerebral cortex from experiment in E. Error bars indicate s.e.m. of nine sections from three independent experiments. Two-way ANOVA revealed a significant difference among different infections, *P<0.05 and ***P<0.001.

Development (2017) 144, 4114-4124 doi:10.1242/dev.156752

examined well-established layer markers. We used layer-specific neuronal markers Tbr1 and Ctip2 to label layers V-VI, and Cux1 to label layers II-IV (Hevner et al., 2001; Nieto et al., 2004). DENV2 infection resulted in a significant decrease in total Tbr1-, Ctip2- and Cux1-labeled neurons compared with controls, but this decrease was far more severe after MEX1-44 infection (Fig. 2E,F). Layer organization appeared normal in both groups of virally infected brains (Fig. 2E). Together, these data suggest that MEX1-44 causes more severe neuronal loss in individual layers compared with DENV2, but neither virus dramatically disrupts layer organization in the developing cerebral cortex.

Asian lineage ZIKV causes more severe disruption of NPCs and neuronal death than DENV2 in the developing brain

To determine why MEX1-44 causes more severe microcephaly than DENV2, we performed a side-by-side comparison of the growth of these two viruses in the developing brain by measuring viral titers. Statistical analyses showed that DENV2 viral titer was significantly

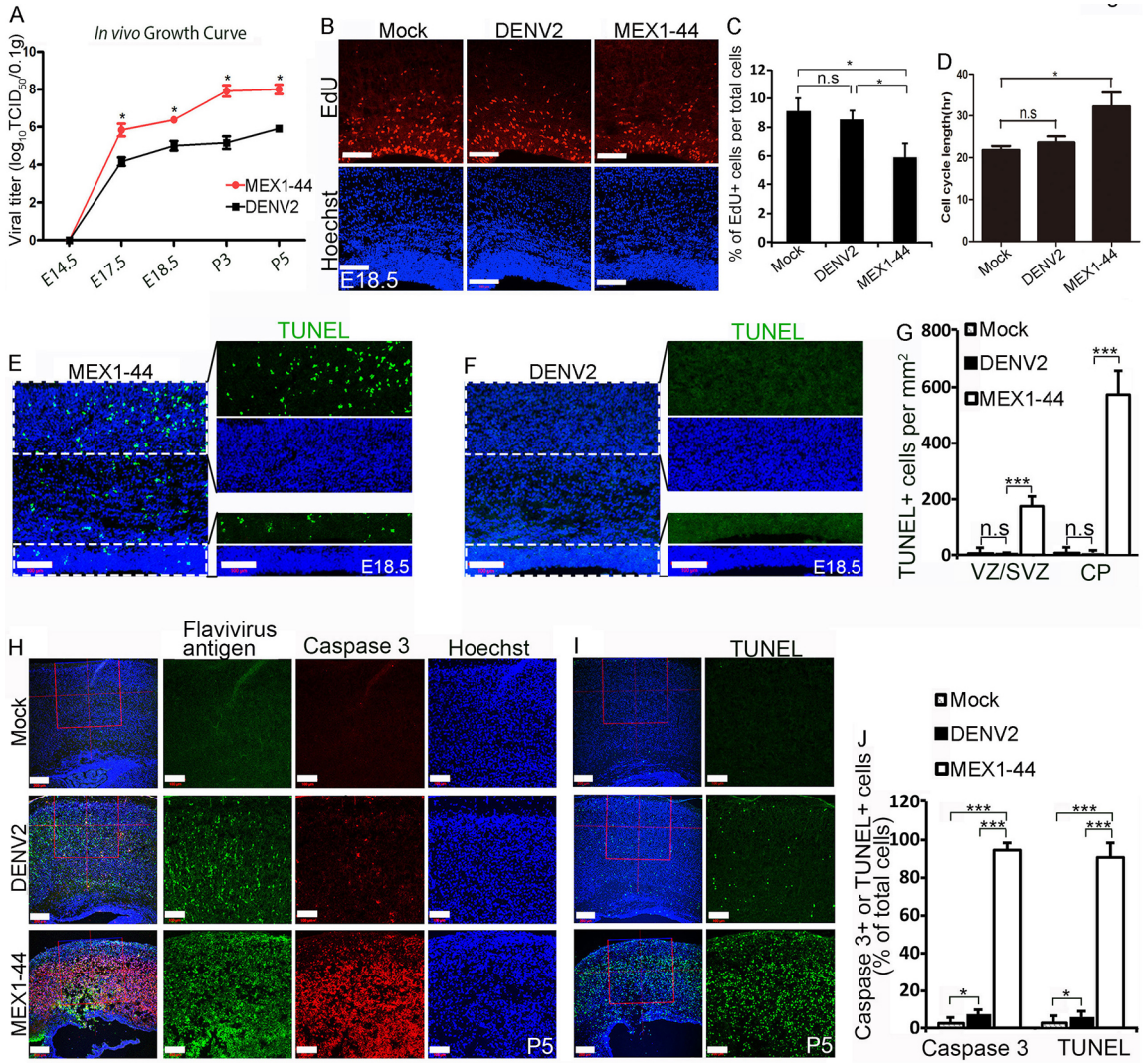

Fig. 3. MEX1-44 causes more severe disruption of NPCs and neuronal death than DENV2 in the developing brain. (A) *In vivo* growth analysis in the developing brain. Viral titers were determined in different stage brains using the TCID50 assay. Error bars indicate the s.e.m. of three independent measurements. ANOVA detected a significant increase in viral titer as development proceeded, **P*<0.05. (B) Confocal micrographs of E18.5 coronal sections with EdU-positive cells after a 45 min EdU pulse. Hoechst stains nuclei (blue). Scale bars: 100 µm. (C) Quantification of the percentage of EdU-positive cells out of total cells in a 1.76×10^5 µm^2 area from experiment in B. Error bars indicate s.e.m. of nine sections from three independent experiments. Two-way ANOVA revealed a significant difference between MEX1-44 and mock, as well as between MEX1-44 and DENV2, but no significant difference between mock and DENV2, **P*<0.05. (D) Quantification of cell cycle length of NPCs in the ventricular/subventricular zone (VZ/SVZ) of E18.5 cerebral cortex. Error bars indicate s.e.m. of nine sections from three independent experiments. Two-way ANOVA revealed a significant difference between MEX1-44 and mock, but no significant difference between mock and DENV2, **P*<0.05. (E,F) TUNEL staining (green) revealed substantial apoptotic cell death in MEX1-44 (E)- but not DENV2 (F)-infected E18.5 cortex. Hoechst stains nuclei (blue). Scale bar: 100 µm. (G) Quantification of the TUNEL-positive cells per mm^2 from a 4.76×10^4 µm^2 VZ/SVZ area or a 1.14×10^5 µm^2 cortical plate (CP) area. Error bars indicate s.e.m. of nine sections from three independent experiments, ****P*<0.001 (Student's *t*-test). (H) Confocal imaging of P5 cerebral cortex stained with antibodies against Flavivirus group antigen (labeling both DENV2 and MEX1-44, green) and cleaved caspase 3 (red). Hoechst stains nuclei (blue). Rightmost three panels are enlargements of the regions outlined by red boxes in the left panels. Scale bars: 200 µm (left panels); 100 µm (right panels). (I) TUNEL staining (green) of coronal sections of P5 cerebral cortex. Hoechst stains nuclei (blue). Right panels are enlargements of the regions outlined by red boxes in the left panels. Scale bars: 200 µm (left panels); 100 µm (right panels). (J) Quantification of the percentage of caspase 3 and TUNEL-positive cells out of total cells in a 4.113×10^5 µm^2 boxed area in experiments in H and I. Two-way ANOVA revealed a significant difference between different viral infections, **P*<0.05 and ****P*<0.001.

Development (2017) 144, 4114-4124 doi:10.1242/dev.156752

lower than that of MEX1-44 (Fig. 3A). Therefore, DENV2 grew less effective in the developing brain compared with MEX1-44. We reasoned that viral growth itself is not sufficient to account for the substantial difference in microcephaly caused by these two viruses, given the extensive DENV2 infection in the developing brain at P5 (Fig. S2A). As NPC disruption leads to microcephaly (Nigg and Raff, 2009; Thornton and Woods, 2009), we hypothesized that MEX1-44 is more potent in disrupting NPCs than DENV2. To test this hypothesis, we examined cell cycle progression and survival of NPCs. Compared with DENV2, MEX1-44 infection caused a reduced S-phase progression of NPCs, based on EdU labeling studies (Fig. 3B,C); and an increase in the percentage of p-Histone3 (p-H3)- and Ki67-positive cells in the VZ/SVZ of the developing cortex (Fig. S5). These results suggest that MEX1-44 caused cell cycle arrest to a significantly higher degree than DENV2, which was further supported by cell cycle length analyses (Fig. 3D). Next, we measured death of NPCs, as MEX1-44 is already known to induce apoptosis of NPCs (Shao et al., 2016). We did not detect apoptotic cells in the mock-treated controls, and TUNEL-positive cells were rarely found in the VZ/SVZ of DENV2-infected brains (Fig. 3F,G). In contrast, there was a substantial population of TUNEL-positive cells in the VZ/SVZ of MEX1-44-infected brains (Fig. 3E,G). Together, these results suggest that Asian lineage ZIKV (MEX1-44) causes a more potent infection, cell cycle arrest and cell death of NPCs than DENV2, resulting in more severe disruption of NPCs.

ZIKV (MEX1-44) infection leads to extensive neuronal death in the developing brain, which contributes to the microcephaly phenotype (Shao et al., 2016). Next, we compared neuronal death induced by MEX1-44 and DENV2. We examined the P5 cortical plate (CP) after intracerebral inoculation of E14.5 brains. Whereas cell death was rarely detected in mock-treated controls, MEX1-44 infection led to the massive neuronal death, reflected by strong caspase 3 and TUNEL staining (Fig. 3H,I). DENV2 also induced a significant increase in neuronal death, but to a much lesser degree than MEX1-44 (Fig. 3H-J). Together, these results suggest that Asian lineage ZIKV (MEX1-44) causes more pronounced apoptosis than DENV2, leading to more severe brain size reduction.

African lineage ZIKV (MR-766) causes more severe neuronal reduction, brain damage and postnatal mortality than Asian lineage ZIKV (MEX1-44)

Although there is no scientific documentation of MR-766-related birth defects, *in vitro* and *ex vivo* studies suggest that MR-766 causes cell cycle arrest and apoptosis of NPCs (Cugola et al., 2016; Simonin et al., 2016; Tang et al., 2016). To determine the effects of MR-766 infection in the developing brain, we performed intracerebral inoculation with ∼1 µl 3.4×10^5 TCID50/ml virus per injection. Surprisingly, we were unable to recover postnatal pups alive; viral infection consistently led to lethality before or around birth (Fig. 4A). We dissected P0 virally infected brains and found a slightly reduced brain size with obvious vasculature abnormalities (Fig. 4B,C). MR-766-infected brains also exhibited severe edema, resulting in fragile brain tissues that could not be used for pathological analyses.

To directly compare the MR-766 and MEX1-44 ZIKV lineages, we performed a side-by-side analysis after intracerebral inoculation of E14.5 brains (Fig. 4D). We focused our analyses at stage E18.5 when living brain tissues can reliably be recovered. No obvious morphological differences were detected between infection groups. However, Hematoxylin and Eosin staining revealed that MR-766 caused cortical thinning with enlarged ventricles, which were not detected in the MEX1-44- or mock-treated brains (Fig. 4E). In addition, MR-766-infected brains exhibited an obvious defect in cortical structural integrity (Fig. 4E, insets), suggesting severe parenchymal cell loss. To directly compare the long-term consequence of viral infection, we performed animal survival analyses. Mock and DENV2-infected pups exhibited no postnatal lethality and survived for at least 2 months after birth, whereas MEX1-44-infected pups did not survive beyond P10, which is consistent with our previous publication (Shao et al., 2016). MR-766 infection resulted in early lethality around P0/P1 with 100% penetrance (Fig. 4F). Together, these results suggest that MR-766 causes more severe brain damage and postnatal mortality than MEX1-44 or DENV2.

Hematoxylin and Eosin staining results suggested that MR-766 infection led to substantial cell loss in the developing brain (Fig. 4E, inset). Next, we examined the neuronal population of the cortex using antibodies against NeuN (Mullen et al., 1992). Although both ZIKV strains caused a substantial reduction in neurons compared with controls, MR-766 infection resulted in a near elimination of the NeuN-positive cells by E18.5 (Fig. 5A,B). To investigate whether layer organization was disrupted by the viral infection, we examined layer markers as described above. We barely detected Tbr1-positive cells in MR-766-infected cerebral cortex at E18.5 (Fig. 5C,D). Compared with MEX1-44, MR-766 caused significantly larger decreases in total Tbr1-, Ctip2- and Cux1-labeled neurons (Fig. 5C,D). Again, layer organization was not severely disrupted. Together, these data suggest that the African lineage ZIKV MR-766 causes more severe neuronal reduction than Asian lineage ZIKV MEX1-44.

African lineage ZIKV (MR-766) induces microglial activation and astrogliosis, and grows faster than Asian lineage ZIKV (MEX1-44)

To understand the mechanisms underlying the differential virulence of MR-766 and MEX1-44, we examined their growth *in vitro* and *in vivo*. Viral titer measurement at 72 h post-infection of cultured human NPCs revealed that there was significantly more growth of MR-766 than of MEX1-44 (Fig. 6A). *In vitro* growth curve analyses showed that MR-766 grew faster than MEX1-44 from day 1 to day 3, although they exhibited similar viral titers from day 4 to day 6 (Fig. 6B), likely due to saturation. After intracerebral inoculation of E14.5 brains, we detected a higher viral titer of MR-766 relative to MEX1-44 in E18.5 brains (Fig. 6C). *In vivo* growth curve analyses showed that MR-766 amplified faster than MEX1-44 in the developing brains (Fig. 6D).

ZIKV infection triggers an innate immune response in the developing brain (Shao et al., 2016; Tang et al., 2016), which can restrict viral infection. However, ZIKV can also suppress the antiviral response of the host (Kumar et al., 2016). To determine whether MR-766 grows faster than MEX1-44 because it can more effectively dampen the host immune response, we examined virus-triggered immune response in the developing cortex. We used antibodies against Iba1 and GFAP to label microglia and astrocytes, respectively (Shao et al., 2016). Whereas both viruses induced microglial activation and astrogliosis (Fig. 6E), there was no significant difference in the percentages of Iba1- and GFAP-positive cells between two virally infected brains (Fig. 6E-G). These results suggest that differential host immune response may not be the major cause of the differences in brain damage induced by these two viruses.

African lineage ZIKV (MR-766) causes more aggravated cell death in NPCs and neurons than Asian lineage ZIKV (MEX1-44)

ZIKV infection results in cell death of NPCs and neurons in the developing brain (Shao et al., 2016; Tang et al., 2016). To investigate why MR-766 caused more severe neuronal loss and brain damage than MEX1-44, we tested the hypothesis that MR-766

Development (2017) 144, 4114-4124 doi:10.1242/dev.156752

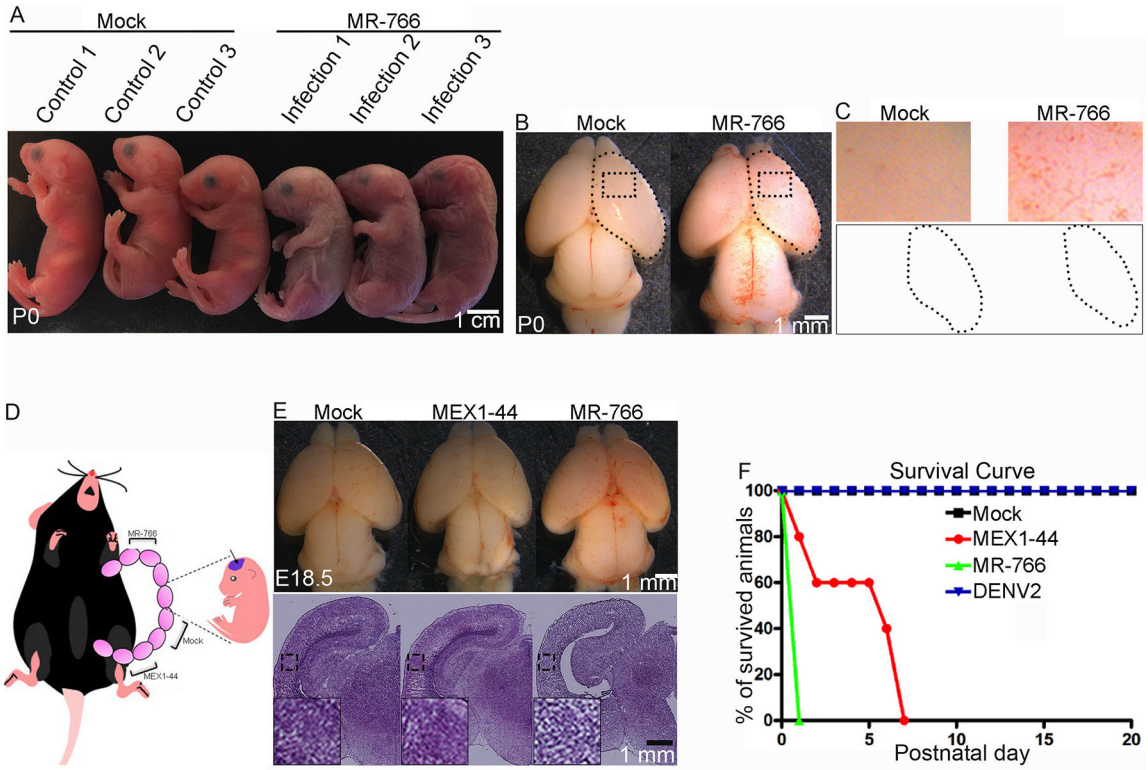

Fig. 4. MR-766 causes more severe brain damage and postnatal death than MEX1-44. (A) Dorsal views of postnatal day 0 (P0) pups. ~1 µl 3.4×10^5 TCID50/ml MR-766 was injected into cerebral ventricles of embryonic day 14.5 (E14.5) brains. Scale bar: 1 cm. (B) Dorsal views of P0 brains after intracerebral inoculation of E14.5 mouse brains with MR-766. Scale bar: 1 mm. Upper panels in C are enlargements of the regions with back dotted rectangles in B; lower panels in C represent a slightly reduced cortex surface after MR-766 infection. (D) Experimental strategies of intracerebral inoculation of embryonic brains with mock treatment, MEX1-44 or MR-766. (E) Dorsal view of E18.5 brain (upper panels). ~1 µl 3.4×10^5 TCID50/ml MEX1-44 or MR-766 were injected into E14.5 cerebral ventricles followed by analyses at E18.5. Hematoxylin and Eosin staining revealed that MR-766 infection resulted in an enlarged ventricle and thinning radial cortex with substantial empty spaces (lower panels). Lower left panels represent enlarged areas from black dotted areas in the middle of the cortex. Scale bar: 1 mm. (F) Survival curves for control (mock), MEX1-44-, MR-766- and DENV2-infected pups. ~1 µl 3.4×10^5 TCID50/ml MEX1-44, MR-766 or DENV2 were injected into cerebral ventricles of E14.5 brains. All the pups were monitored daily from postnatal day 0 to 20, and surviving DENV2-infected pups were observed until 2 months of age. The percentage of survival was calculated, and the survival curves represent three independent experiments (n=10).

is more potent in causing death of NPCs and neurons than MEX1-44. We infected human NPCs and then performed cell death analyses, in which antibodies against Sox2 and caspase 3 were used to label NPCs and apoptotic cells, respectively (Fig. 7A). Statistical analysis showed that MR-766 infection resulted in a larger percentage of apoptotic NPCs compared with MEX1-44 (Fig. 7B). These results suggest that MR-766 is more potent in causing death of NPCs than MEX1-44 *in vitro*.

Next, we compared NPC and neuronal death induced by ZIKV *in vivo*. We examined E18.5 cerebral cortex after intracerebral inoculation of E14.5 embryonic brains. Whereas cell death was rarely detected in mock controls, MEX1-44 infection led to substantial cell death in both the VZ/SVZ and cortical plate, reflected by caspase 3 and TUNEL staining (Fig. 7C-F). Strikingly, MR-766 infection resulted in a much more dramatic increase in caspase 3- and TUNEL-positive cells in the developing brain compared with MEX1-44 (Fig. 7C-F). Together, these results suggest that MR-766 causes more pronounced death of NPCs and neurons than MEX1-44, which is likely why MR-766 infection causes more severe neuronal loss and brain damage.

DISCUSSION

In this work we found that DENV2 is sufficient to cause microcephaly due to increased cell death in neural progenitor cells (NPCs) and neurons. However, DENV2 infection has minimal detrimental effects on the developing brain and pups can ultimately survive embryonic infection. By performing side-by-side intracerebral inoculation, we discovered that the African lineage ZIKV (MR-766) causes more severe brain damage and postnatal lethality than currently circulating Asian lineage ZIKV (MEX1-44). MR-766 grows faster and causes more severe neuronal death in the developing brain, contributing to earlier lethality compared with MEX1-44.

The finding that African linage ZIKV (MR-766) causes severe brain damage is supported by multiple analyses, including animal survival studies, *in vitro* and *in vivo* viral growth assays, NPC and neuronal death assays, and cortical neuron number analyses. Based on studies using NPCs derived from human ES cells or iPS cells, it had remained unclear whether African lineage isolates exhibit a stronger detrimental effect on NPCs compared with Asian lineage isolates (Cugola et al., 2016; Simonin et al., 2016). It has been reported that MR-766 infection results in larger neurospheres than an Asian lineage isolate, which seemed to favor the hypothesis that African lineage ZIKV is less potent in damaging NPCs (Cugola et al., 2016). These observations are consistent with the fact that there is no scientific documentation of ZIKV-Africa-related birth defects. Here, our *in vivo* studies revealed that African lineage ZIKV (MR-766) is more virulent and causes more severe mortality and brain damage than currently circulating Asian lineage (MEX1-44). Because the MR-766 strain has been adapted to the mouse brain for

Development (2017) 144, 4114-4124 doi:10.1242/dev.156752

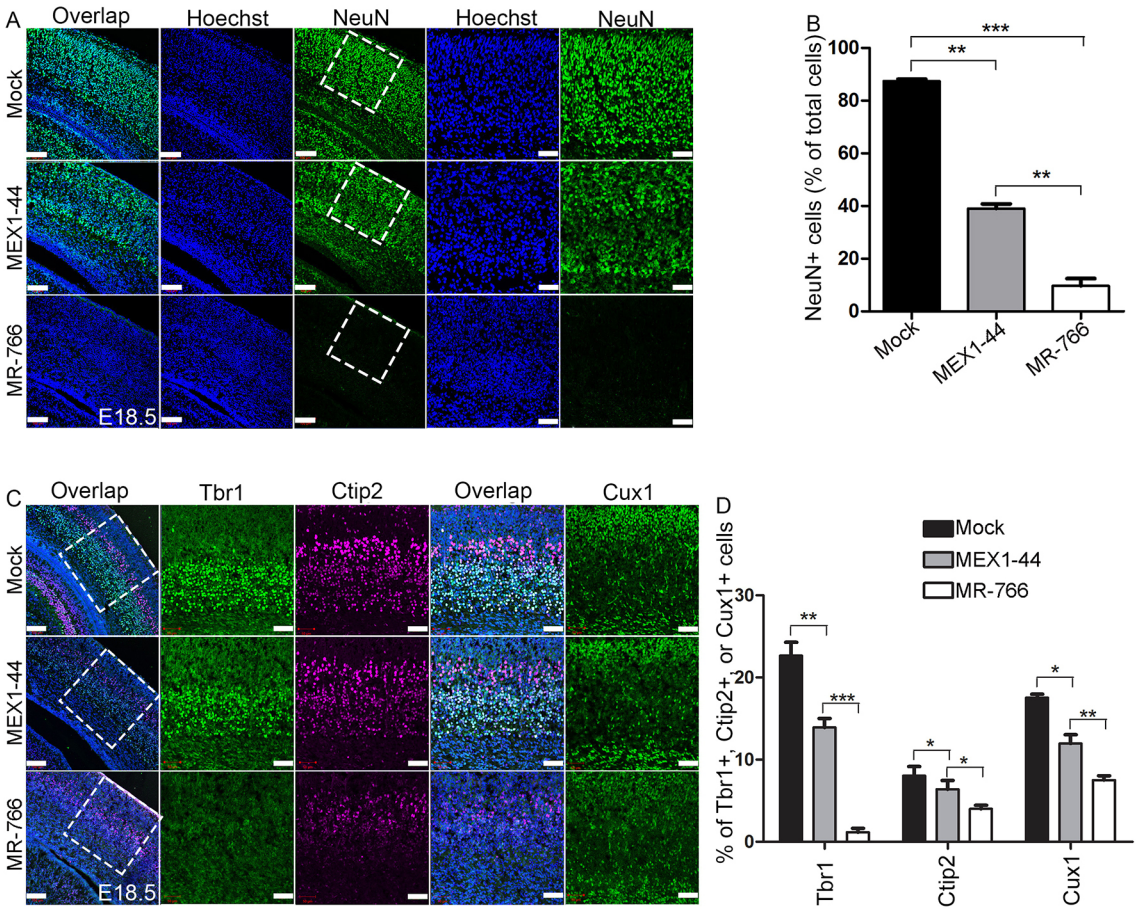

Fig. 5. More neuron loss in MR-766 infected brains compared with MEX1-44. (A) Confocal imaging of E18.5 cerebral cortex stained with antibodies against NeuN (green). The two rightmost panels represent enlargements of areas outlined with white dotted boxes. Hoechst stains nuclei (blue). Scale bars: 100 µm (left panels); 50 µm (right panels). (B) Quantification of the percentage of NeuN-positive cells out of total cells within a 4.0×10^4 µm^2 cortical plate areas in A. Error bars indicate s.e.m. of nine sections from three independent experiments. Two-way ANOVA revealed a significant difference among different infections, $^{**}P<0.01$ and $^{***}P<0.001$. (C) Confocal microscope images of coronal sections from E18.5 cortex stained with antibodies against Ctip2 (purple), Tbr1 (green) and Cux1 (green). Hoechst stains nuclei (blue). Rightmost four panels are enlargements of the regions outlined by red boxes in the left panels. Scale bars: 100 µm (left panels); 50 µm (right panels). (D) Quantification of the percentage of Ctip2-, Tbr1- and Cux1-positive cells out of total cells in the boxed areas of E18.5 cerebral cortex from experiment in C. Error bars indicate s.e.m. of nine sections from three independent experiments. Two-way ANOVA revealed a significant difference among different infections, $^{*}P<0.05$, $^{**}P<0.01$ and $^{***}P<0.001$.

many generations, our studies cannot yet draw a broad generalization that the African lineage of ZIKV is more virulent than the Asian lineage. However, using a low-passage, currently circulating African ZIKV strain, recent studies have reported that an African lineage isolate exhibited a higher infection rate and caused a higher degree of cell death in NPCs than an Asian lineage isolate (Simonin et al., 2016). In addition, studies by Shashank Tripathi et al. have reported that two African strains, the Senegal 1984 Strain DAKAR 41519 and Uganda 1947 Strain MR 766, have similar virulence and both cause more severe weight loss and mortality than Asian strains, including Puerto Rico 2015 (Strain PRVABC59), Cambodia 2010 (Strain FSS13025) and Malaysia 1966 (Strain P6-740) (Tripathi et al., 2017). Our results focusing on the developing brain complement these studies, collectively suggesting that African lineage ZIKV is more virulent and causes more severe mortality and brain damage than the Asian lineage ZIKV.

Future studies should identify molecular mechanisms underlying this differential virulence between the African lineage and Asian lineage. It will be important to know whether African isolates are more effective in binding, entering or replicating in human NPCs, and whether they cause more pronounced cell cycle arrest of NPCs compared with Asian lineage isolates (Li et al., 2016; Shao et al., 2016). It has been reported that an Asian lineage isolate, but not MR-766, upregulates TP53 and viral response genes in human NPCs (Zhang et al., 2016). It will be informative to test whether the different virulence capacities of these two ZIKV strains are due to the differential induction of TP53 in the developing brain. Our functional studies of different ZIKV strains should provide a baseline for investigating how genetic changes in different ZIKV strains affect their pathogenesis in the developing brain. In the future, it will be important to use a reverse genetics systems for Asian and African Zika viruses to generate inter-lineage chimeric viruses followed by functional studies, which should facilitate the studies of ZIKV pathogenesis in the developing brain (Atieh et al., 2016; Gadea et al., 2016).

We found that DENV2 infection is sufficient to cause microcephaly and global growth restriction. DENV2 infects human and mouse NPCs, which is consistent with previous publications in hNPCs (Garcez et al., 2016). DENV2 infection causes a significant increase in cell death in NPCs and neurons, resulting in smaller brain sizes. Interestingly, microcephaly in DENV2-infected pups was accompanied by global growth restriction, which was also observed in ZIKV (MEX1-44)-infected pups (Shao et al., 2016). In addition to

Development (2017) 144, 4114-4124 doi:10.1242/dev.156752

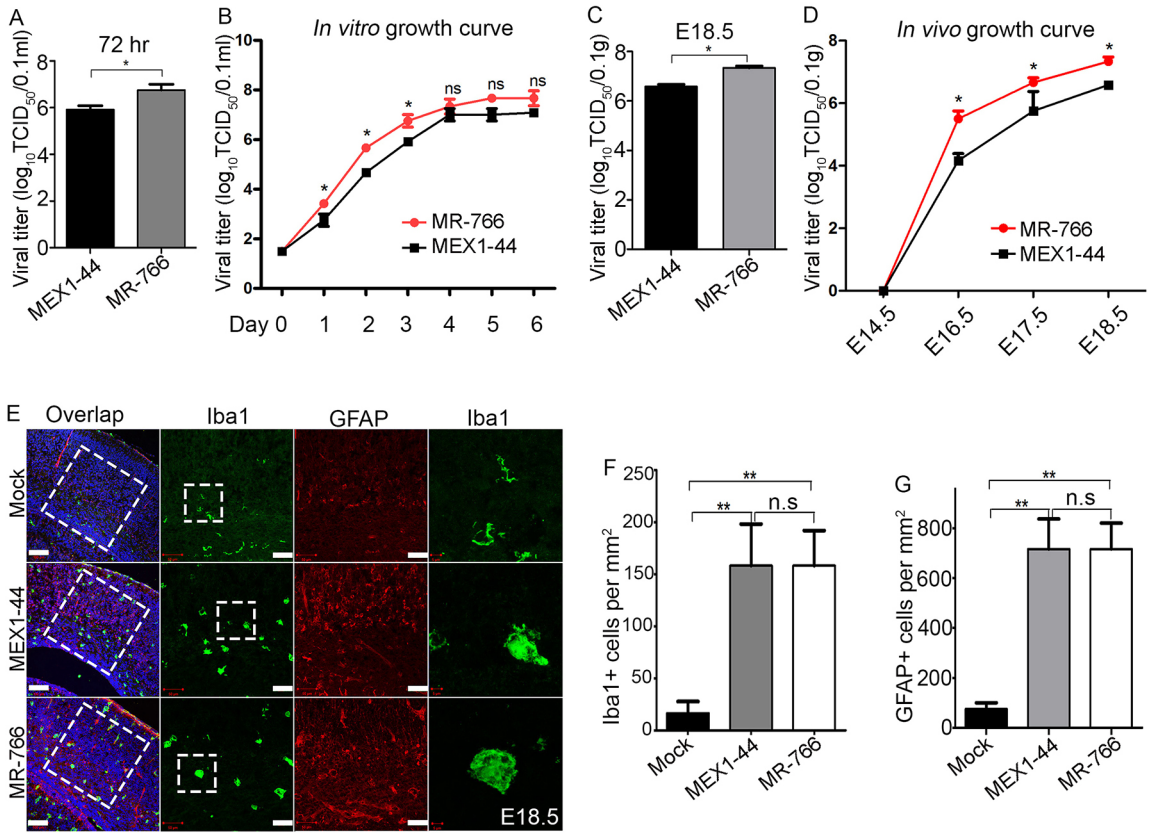

Fig. 6. MR-766 grows faster than MEX1-44 and triggers a similar immune response. (A) Quantification of the viral titers at 72 h after MEX1-44 or MR-766 infection of human neural progenitor cells (hNPCs). Error bars indicate the s.e.m. of three independent measurements. **P*<0.05 (Student's *t*-test). (B) *In vitro* growth analysis of viral infection in cultured hNPCs. Viral titers were determined on different days, as indicated using the TCID50 assay. Error bars indicate the s.e.m. of three independent measurements. ANOVA revealed that MR-766 exhibited a higher rate of growth than MEX1-44 from post-infection day 1 to 3. **P*<0.05; ns, not significant. (C) Quantification of the viral titers at E18.5 after MEX1-44 or MR-766 infection of E14.5 embryonic brains. Error bars indicate the s.e.m. of three independent measurements. **P*<0.05 (Student's *t*-test). (D) *In vivo* growth analysis in the developing brain. Viral titers were determined at different stage brains using the TCID50 assay. Error bars indicate the s.e.m. of three independent measurements. ANOVA detected a significant difference between the viral titers at each developmental stage, **P*<0.05. (E) Confocal micrographs of coronal sections of the E18.5 cerebral cortex stained with antibodies against GFAP (red) and Iba1 (green). Hoechst stains nuclei (blue). Scale bars: 100 µm (left); 50 µm (middle); 10 µm (right). Rightmost panels are enlargements of white dotted areas in the second panels. (F,G) Quantification of Iba1- or GFAP-positive cells per mm^2 area. Two-way ANOVA revealed a significant difference between ZIKV and control groups, but no significant difference was detected between MR-766 and MEX1-44. ***P*<0.001; ns, no significant difference.

its specific damage to the brain, intracerebral inoculation of viruses could have an adverse impact on global growth due to inflammation and the immune response of the fetus during development. Our results suggest that DENV2 is intrinsically less potent in damaging the developing brain than ZIKV; however, our studies cannot rule out any long-term potential neurological deficiencies in these DENV2-infected pups. It has been reported that antibodies against E protein domain I/II (EDI/II) of ZIKV lethally enhanced DENV disease in mice (Stettler et al., 2016). Future studies should determine whether immunity to ZIKV could exacerbate brain damage derived from DENV infection.

MATERIALS AND METHODS

Ethics statement

All animals were handled according to protocols approved by the Institutional Animal Care and Use Committee (IACUC) at the University of Georgia (UGA). All of the experiments related to ZIKV and DENV2 were conducted following protocols approved by the UGA Institutional Biosafety Committee.

Viruses

DENV2, strain S16803 (GenBank GU289914), was isolated from a patient sample from Thailand in 1974 and passaged in C6/36 cells. The virus was passaged twice in Vero cells by the World Reference Center for Emerging Viruses and Arboviruses (WRCEVA) before mouse injections. ZIKV MEX1-44 was isolated in Chiapas, Mexico in January of 2016 from an infected *Aedes aegypti* mosquito. The virus was passaged by WRCEVA four times in Vero cells. We obtained this virus, with permission, through the University of Texas Medical Branch at Galveston (UTMB). We then amplified the stock an additional two passages in Vero cells, so the virus used in the experiments had been passaged six times in Vero cells from the time it was isolated from the mosquito. MR-766 is a Zika virus stock from the initial Zika virus isolation from a sentinel rhesus monkey in 1947 from Uganda. The viral stock was passaged numerous times in mouse brain and Vero cell culture. Stock was provided by ATCC (ATCC VR-84). Designated tools and surfaces exposed to ZIKV or DENV2 were disinfected with 10% bleach to destroy remaining viral particles after use. All tissues used for histology were fixed in 4% PFA to inactivate the viruses for analysis.

Viral inoculation of embryonic brains

For timed pregnant mating, noon of the day after mating was considered embryonic day 0.5 (E0.5). Pregnant C57BL/6J or 129 mice with E14.5 embryos were treated with ketamine hydrochloride and xylazine to induce anesthesia. ~1 µl 3.4×10^5 TCID50/ml ZIKV (MEX-1-44 or MR766) or DENV2 (strain S16803) were injected into the lateral ventricles of E14.5 embryo brains. Control media was used as a sham injection. Injected embryos were placed back into pregnant dams and allowed to develop after surgery for varying periods of time according to the individual experiments.

Development (2017) 144, 4114-4124 doi:10.1242/dev.156752

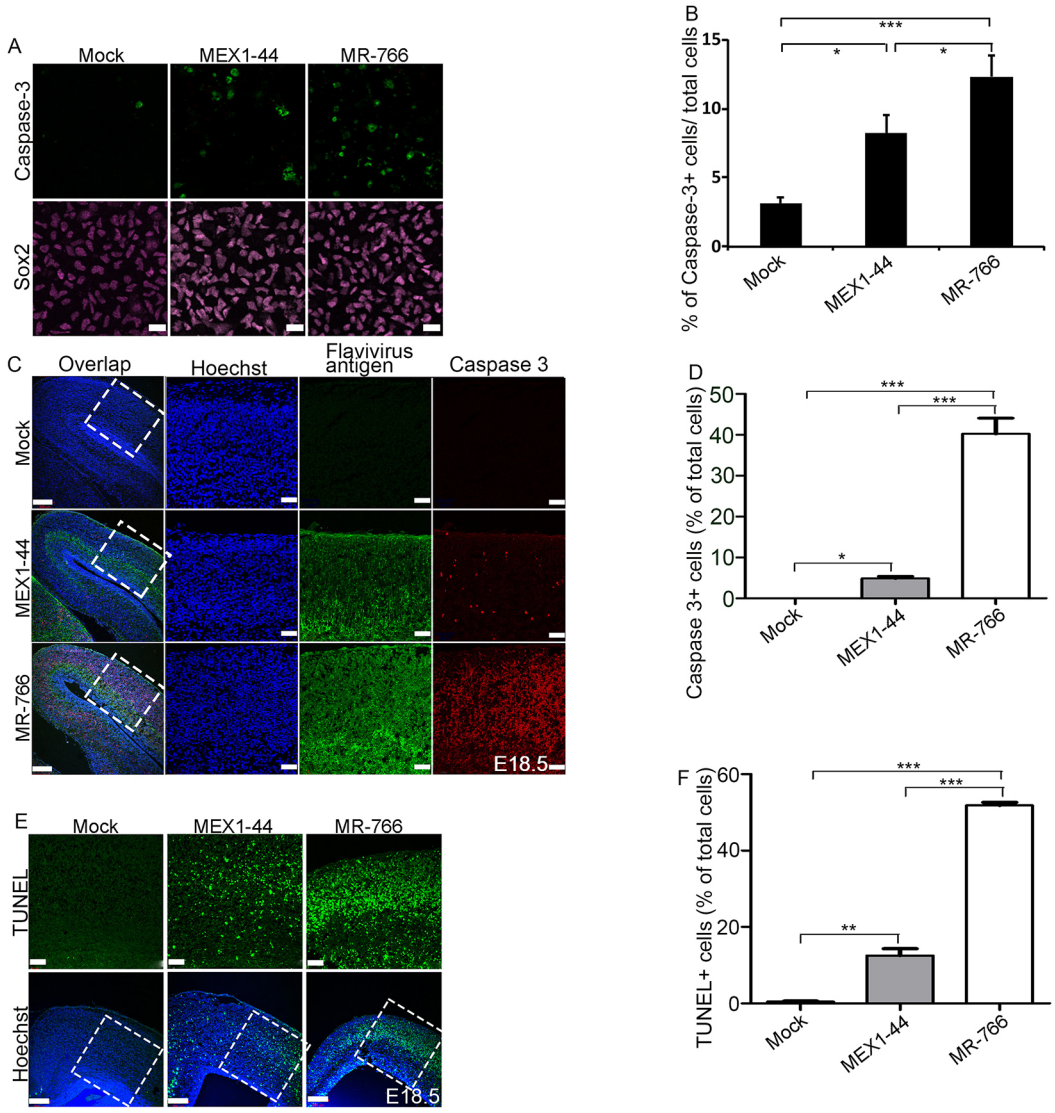

Fig. 7. MR-766 infection leads to more cell death in NPCs and neurons than MEX1-44. (A) Confocal imaging of human neural progenitor cells (hNPCs) stained with antibodies against Sox2 (purple) or caspase 3 (green). Scale bars: 20 µm. (B) Quantification of the percentage of caspase 3-positive cells out of total hNPCs. Error bars indicate s.e.m. of results from three independent experiments. Two-way ANOVA revealed a significant difference between mock, MEX1-44 and MR-766 (*P<0.05, ***P<0.001). (C) Confocal imaging of E18.5 cerebral cortex stained with antibodies against Flavivirus antigen (labeling MR-766 or MEX1-44, green) and caspase 3 (red). Hoechst stains nuclei (blue). Rightmost three panels are enlargements of the regions outlined by white dotted boxes in the left panels. Scale bars: 200 µm (left panels); 50 µm (right panels). (D) Quantification of the percentage of caspase 3-positive cells out of total cells. Two-way ANOVA revealed a significant difference between different treatments, *P<0.05 and ***P<0.001. (E) TUNEL staining (green) on coronal sections of E18.5 brains. Hoechst stains nuclei (blue). Upper panels are enlargements of the regions outlined by white dotted boxes in lower panels. Scale bars: 50 µm (upper panels); 200 µm (lower panels). (F) Quantification of the percentage of TUNEL-positive cells out of total cells. Two-way ANOVA revealed a significant difference between different treatments, **P<0.01 and ***P<0.001.

Virus titration

Vero cells (African green monkey kidney epithelial cells) were obtained from ATCC. Vero cells were maintained in Dulbecco's modified Eagle's medium (DMEM) supplemented with penicillin/streptomycin and 10% fetal bovine serum (FBS) at 37°C with 5% CO_2. ZIKV or DENV2 stocks were propagated on Vero cells after inoculating at a multiplicity of infection of 0.01 and harvesting supernatants at 96 h and 120 h post-infection. The viral titers for brains were determined as 50% tissue culture infectious doses (TCID50) on Vero cells. Briefly, brain tissues were homogenized in 10 volumes of PBS and centrifuged at 3000 rpm for 10 min. The supernatant was serially diluted 10-fold in DMEM. A 100 µl aliquot of each diluted sample was added to 96-well plates containing a monolayer of Vero cells. Cells were cultured for 96-120 h at 37°C in a tissue culture incubator. Cytopathic effect (CPE) of endpoint dilutions was monitored.

Mouse brain phenotype analysis

Histological processing, TUNEL assay and immunohistochemical labeling of cryosections were performed as described previously (Chen et al., 2014). Coronal sections of the cerebral cortex from different stages of embryos were used as indicated in the figures and text. The primary antibodies used are listed in Table S1. The secondary antibodies used were Alexa 488 and Alexa 555 conjugated to specific IgG types (Invitrogen Molecular Probes). All the experiments were repeated at least three times, and representative images are shown in the individual figures.

EdU and CldU labeling study

After ZIKV or DENV2 inoculation of E14.5 brains, pregnant dams with E18.5 embryos were injected intraperitoneally with EdU (1 mg/ml, Invitrogen, 100 µl per 100 g body weight) or CldU (10 mg/ml, Sigma,

Development (2017) 144, 4114-4124 doi:10.1242/dev.156752

100 µl for per 100 g body weight). The animals were sacrificed 45 min (for EdU) or 2 h (for CldU) after the injection. The brains were dissected and fixed in 4% paraformaldehyde (PFA) overnight. Subsequently, the brains were stored in 30% sucrose for 16 h and embedded in Tissue-Tek OCT Compound (Sakura). For EdU staining, cortical coronal sections were prepared for staining using Click-iT plus EdU proliferation kit (Invitrogen). For CldU staining, cortical coronal sections were stained with antibody against CldU (Abcam, ab6326).

Cell cycle length analysis

Cell cycle kinetics were determined using a dual labeling approach as described previously (Martynoga et al., 2005; Shao et al., 2016). On embryonic day 18.5, the pregnant mouse was injected with CldU (10 mg/ml, Sigma, 100 ul for per 100 g body weight) at a time designated as T=0 h, such that all cells at S phase from the beginning of the experiment were labeled with CldU. At T=1.5 h, the pregnant mouse was injected with EdU (1 mg/ml, Invitrogen, 100 ul for per 100 g body weight) to label all cells in S-phase. The animal was killed at T=2 h and its embryos were collected immediately. Embryo sections were immunostained by an Anti-CldU antibody (Abcam, ab6326) and Click-iT EdU Alexa Fluor 555 imaging Kit (Life Technologies, C10338). Images were obtained on a Zeiss LSM 710 inverted confocal microscope. The length of S-phase (Ts) and total length of cell cycle (Tc) was determined based on the relative number of cells that incorporated CldU or EdU (Martynoga et al., 2005), or both. The ratio of the length of any one period of the cell cycle to that of another period is equal to the ratio of the number of cells in the first period to the number in the second period (Nowakowski et al., 1989). Thus, the length of S phase (Ts) was calculated as the interval between both injections (Ti=1.5 h) divided by the quotient of the density of $CldU^{+}EdU^{-}$ cells (cells that were in but left S phase before EdU injection) and $CldU^{+}EdU^{+}$ cells (cells remaining in S phase at the end of the experiment). Ti/Ts=Lcells/Scells (Ti=1.5; Lcells=$CldU^{+}EdU^{-}$; Scells=$CldU^{+}EdU^{+}$). Using the same logic, the total cell cycle length can be calculated as: Ts/Tc=Scells/Pcells (Tc: total cell cycle length; Pcells is estimated by counting the total numbers of cells in the assessed area).

In vitro infection and immunofluorescence

hNP1 Human Neural Progenitor Cells (ArunA Biomedical, derived from the WA09 human embryonic stem cells) were infected with MEX1-44, MR-766 or mock (cultured medium from Vero cells). 1.8×10^{5} cells seeded in four-well chamber slides were cultured for 24 h followed by virus infection (MOI=0.5, 1, 10, and 20). The infection conditions were 37°C for 2 or 6 h. Next, the inoculum was removed and cells were washed twice with DPBS (Hyclone) followed by fresh medium addition. After 72 h, cells were fixed with 4%, paraformaldehyde for 10 min at room temperature. After blocking with 0.2% Triton X-100 and 10% goat serum in PBS, the cells were incubated with primary antibodies overnight at 4°C followed by incubation with secondary antibodies for 1 h at room temperature. Primary and secondary antibodies were diluted with 0.2% Triton X-100 and 2% BSA in PBS. Hoechst 33342 was added together with secondary antibodies at 1 µl/ml. The following antibodies were used: anti-Flavivirus group antigen antibody (mouse IgG2a, EMD Millipore, MAB10216; 1:1000), anti-active-caspase-3 (rabbit, BD 559565; 1:800), anti-Sox2 (rat IgG2a, BD14-9811; 1:1000), anti-mouse IgG2a Alexa Fluor 555, anti-rabbit Alexa Flour 488 and anti-rat IgG2a Alexa Fluor 647 (Invitrogen). Images were acquired with a Zeiss 710 confocal microscope. ImageJ was used for analyzing data.

Acknowledgements

We thank Chen lab colleagues for stimulating discussions. We thank Bridget Samuels for critical reading of this manuscript. Zika and dengue virus isolates were provided by the World Reference Center for Emerging Viruses and Arboviruses at The University of Texas Medical Branch.

Competing interests

The authors declare no competing or financial interests.

Author contributions

Conceptualization: Q.S., S.H., J.-F.C.; Methodology: Q.S., S.H., Y.-N.Z., M.Y., F.G., S.L.S., X.-P.Q., M.A.B., J.-F.C.; Formal analysis: Q.S., M.Y.; Investigation: Q.S., S.H., M.Y., F.G., M.A.B.; Data curation: Q.S.; Writing - original draft: J.-F.C.; Writing - review & editing: S.H., J.-F.C.; Project administration: Y.-N.Z.; Funding acquisition: J.-F.C.

Funding

The Chen lab is supported by funds from the National Institutes of Health (R00HD073269, R01NS097231 and R01NS096176 to J.-F.C.). Deposited in PMC for release after 12 months.

Supplementary information

Supplementary information available online at http://dev.biologists.org/lookup/doi/10.1242/dev.156752.supplemental

References

Angevine, J. B. and Sidman, R. L. (1961). Autoradiographic study of cell migration during histogenesis of cerebral cortex in the mouse. *Nature* **192**, 766-768.

Atieh, T., Baronti, C., de Lamballerie, X. and Nougairède, A. (2016). Simple reverse genetics systems for Asian and African Zika viruses. *Sci. Rep.* **6**, 39384.

Barba-Spaeth, G., Dejnirattisai, W., Rouvinski, A., Vaney, M.-C., Medits, I., Sharma, A., Simon-Lorière, E., Sakuntabhai, A., Cao-Lormeau, V.-M., Haouz, A. et al. (2016). Structural basis of potent Zika-dengue virus antibody cross-neutralization. *Nature* **536**, 48-53.

Brasil, P., Pereira, J. P., Moreira, M. E., Ribeiro Nogueira, R. M., Damasceno, L., Wakimoto, M., Rabello, R. S., Valderramos, S. G., Halai, U.-A., Salles, T. S. et al. (2016). Zika virus infection in pregnant women in Rio de Janeiro. *N. Engl. J. Med.* **375**, 2321-2334.

Chen, J.-F., Zhang, Y., Wilde, J., Hansen, K. C., Lai, F. and Niswander, L. (2014). Microcephaly disease gene Wdr62 regulates mitotic progression of embryonic neural stem cells and brain size. *Nat. Commun.* **5**, 3885.

Cugola, F. R., Fernandes, I. R., Russo, F. B., Freitas, B. C., Dias, J. L. M., Guimarães, K. P., Benazzato, C., Almeida, N., Pignatari, G. C., Romero, S. et al. (2016). The Brazilian Zika virus strain causes birth defects in experimental models. *Nature* **534**, 267-271.

Dejnirattisai, W., Supasa, P., Wongwiwat, W., Rouvinski, A., Barba-Spaeth, G., Duangchinda, T., Sakuntabhai, A., Cao-Lormeau, V.-M., Malasit, P., Rey, F. A. et al. (2016). Dengue virus sero-cross-reactivity drives antibody-dependent enhancement of infection with zika virus. *Nat. Immunol.* **17**, 1102-1108.

Dupont-Rouzeyrol, M., O'Connor, O., Calvez, E., Daurès, M., John, M., Grangeon, J.-P. and Gourinat, A.-C. (2015). Co-infection with Zika and dengue viruses in 2 patients, New Caledonia, 2014. *Emerging Infect. Dis.* **21**, 381-382.

Faria, N. R., Azevedo, R. D. S. D. S., Kraemer, M. U. G., Souza, R., Cunha, M. S., Hill, S. C., Thézé, J., Bonsall, M. B., Bowden, T. A., Rissanen, I. et al. (2016). Zika virus in the Americas: early epidemiological and genetic findings. *Science* **352**, 345-349.

Gadea, G., Bos, S., Krejbich-Trotot, P., Clain, E., Viranaicken, W., El-Kalamouni, C., Mavingui, P. and Desprès, P. (2016). A robust method for the rapid generation of recombinant Zika virus expressing the GFP reporter gene. *Virology* **497**, 157-162.

Garcez, P. P., Loiola, E. C., Madeiro da Costa, R., Higa, L. M., Trindade, P., Delvecchio, R., Nascimento, J. M., Brindeiro, R., Tanuri, A. and Rehen, S. K. (2016). Zika virus impairs growth in human neurospheres and brain organoids. *Science* **352**, 816-818.

Haddow, A. D., Schuh, A. J., Yasuda, C. Y., Kasper, M. R., Heang, V., Huy, R., Guzman, H., Tesh, R. B. and Weaver, S. C. (2012). Genetic characterization of Zika virus strains: geographic expansion of the Asian lineage. *PLoS Negl. Trop. Dis.* **6**, e1477.

Hamel, R., Liégeois, F., Wichit, S., Pompon, J., Diop, F., Talignani, L., Thomas, F., Desprès, P., Yssel, H. and Missé, D. (2016). Zika virus: epidemiology, clinical features and host-virus interactions. *Microbes Infect.* **18**, 441-449.

Hevner, R. F., Shi, L., Justice, N., Hsueh, Y.-P., Sheng, M., Smiga, S., Bulfone, A., Goffinet, A. M., Campagnoni, A. T. and Rubenstein, J. L. R. (2001). Tbr1 regulates differentiation of the preplate and layer 6. *Neuron* **29**, 353-366.

Kumar, A., Hou, S., Airo, A. M., Limonta, D., Mancinelli, V., Branton, W., Power, C. and Hobman, T. C. (2016). Zika virus inhibits type-I interferon production and downstream signaling. *EMBO Rep.* **17**, 1766-1775.

Li, C., Xu, D., Ye, Q., Hong, S., Jiang, Y., Liu, X., Zhang, N., Shi, L., Qin, C.-F. and Xu, Z. (2016). Zika virus disrupts neural progenitor development and leads to microcephaly in mice. *Cell Stem Cell* **19**, 672.

Marín, O. and Rubenstein, J. L. R. (2003). Cell migration in the forebrain. *Annu. Rev. Neurosci.* **26**, 441-483.

Marrs, C., Olson, G., Saade, G., Hankins, G., Wen, T., Patel, J. and Weaver, S. (2016). Zika virus and pregnancy: a review of the literature and clinical considerations. *Am. J. Perinatol.* **33**, 625-639.

Martynoga, B., Morrison, H., Price, D. J. and Mason, J. O. (2005). Foxg1 is required for specification of ventral telencephalon and region-specific regulation of dorsal telencephalic precursor proliferation and apoptosis. *Dev. Biol.* **283**, 113-127.

Miner, J. J., Cao, B., Govero, J., Smith, A. M., Fernandez, E., Cabrera, O. H., Garber, C., Noll, M., Klein, R. S., Noguchi, K. K. et al. (2016). Zika virus infection

during pregnancy in mice causes placental damage and fetal demise. *Cell* **165**, 1081-1091.

Mullen, R. J., Buck, C. R. and Smith, A. M. (1992). NeuN, a neuronal specific nuclear protein in vertebrates. *Development* **116**, 201-211.

Nieto, M., Monuki, E. S., Tang, H., Imitola, J., Haubst, N., Khoury, S. J., Cunningham, J., Götz, M. and Walsh, C. A. (2004). Expression of Cux-1 and Cux-2 in the subventricular zone and upper layers II-IV of the cerebral cortex. *J. Comp. Neurol.* **479**, 168-180.

Nigg, E. A. and Raff, J. W. (2009). Centrioles, centrosomes, and cilia in health and disease. *Cell* **139**, 663-678.

Nowakowski, R. S., Lewin, S. B. and Miller, M. W. (1989). Bromodeoxyuridine immunohistochemical determination of the lengths of the cell cycle and the DNA-synthetic phase for an anatomically defined population. *J. Neurocytol.* **18**, 311-318.

Nunes, M. R. T., Faria, N. R., Vasconcelos, H. B., Medeiros, D. B. A., Silva de Lima, C. P., Carvalho, V. L., Pinto da Silva, E. V., Cardoso, J. F., Sousa, E. C., Nunes, K. N. B. et al. (2012). Phylogeography of dengue virus serotype 4, Brazil, 2010-2011. *Emerging Infect. Dis.* **18**, 1858-1864.

Nunes, M. R. T., Palacios, G., Faria, N. R., Sousa, E. C., Pantoja, J. A., Rodrigues, S. G., Carvalho, V. L., Medeiros, D. B. A., Savji, N., Baele, G. et al. (2014). Air travel is associated with intracontinental spread of dengue virus serotypes 1-3 in Brazil. *PLoS Negl. Trop. Dis.* **8**, e2769.

Paniz-Mondolfi, A. E., Rodriguez-Morales, A. J., Blohm, G., Marquez, M. and Villamil-Gomez, W. E. (2016). ChikDenMaZika Syndrome: the challenge of diagnosing arboviral infections in the midst of concurrent epidemics. *Ann. Clin. Microbiol. Antimicrob.* **15**, 42.

Priyamvada, L., Quicke, K. M., Hudson, W. H., Onlamoon, N., Sewatanon, J., Edupuganti, S., Pattanapanyasat, K., Chokephaibulkit, K., Mulligan, M. J., Wilson, P. C. et al. (2016). Human antibody responses after dengue virus infection are highly cross-reactive to Zika virus. *Proc. Natl. Acad. Sci. USA* **113**, 7852-7857.

Shao, Q., Herrlinger, S., Yang, S.-L., Lai, F., Moore, J. M., Brindley, M. A. and Chen, J.-F. (2016). Zika virus infection disrupts neurovascular development and results in postnatal microcephaly with brain damage. *Development* **143**, 4127-4136.

Simonin, Y., Loustalot, F., Desmetz, C., Foulongne, V., Constant, O., Fournier-Wirth, C., Leon, F., Molès, J.-P., Goubaud, A., Lemaitre, J.-M. et al. (2016). Zika virus strains potentially display different infectious profiles in human neural cells. *EBioMedicine* **12**, 161-169.

Stettler, K., Beltramello, M., Espinosa, D. A., Graham, V., Cassotta, A., Bianchi, S., Vanzetta, F., Minola, A., Jaconi, S., Mele, F. et al. (2016). Specificity, cross-reactivity, and function of antibodies elicited by Zika virus infection. *Science* **353**, 823-826.

Swanstrom, J. A., Plante, J. A., Plante, K. S., Young, E. F., McGowan, E., Gallichotte, E. N., Widman, D. G., Heise, M. T., de Silva, A. M. and Baric, R. S. (2016). Dengue virus envelope dimer epitope monoclonal antibodies isolated from dengue patients are protective against Zika virus. *MBio* **7**, e01123-16.

Tang, H., Hammack, C., Ogden, S. C., Wen, Z., Qian, X., Li, Y., Yao, B., Shin, J., Zhang, F., Lee, E. M. et al. (2016). Zika virus infects human cortical neural progenitors and attenuates their growth. *Cell Stem Cell* **18**, 587-590.

Thornton, G. K. and Woods, C. G. (2009). Primary microcephaly: do all roads lead to Rome? *Trends Genet.* **25**, 501-510.

Tripathi, S., Balasubramaniam, V. R. M. T., Brown, J. A., Mena, I., Grant, A., Bardina, S. V., Maringer, K., Schwarz, M. C., Maestre, A. M., Sourisseau, M. et al. (2017). A novel Zika virus mouse model reveals strain specific differences in virus pathogenesis and host inflammatory immune responses. *PLoS Pathog.* **13**, e1006258.

Ventura, C. V., Maia, M., Bravo-Filho, V., Góis, A. L. and Belfort, R. (2016). Zika virus in Brazil and macular atrophy in a child with microcephaly. *Lancet* **387**, 228.

Villamil-Gómez, W. E., Rodríguez-Morales, A. J., Uribe-García, A. M., González-Arismendy, E., Castellanos, J. E., Calvo, E. P., Álvarez-Mon, M. and Musso, D. (2016). Zika, dengue, and chikungunya co-infection in a pregnant woman from Colombia. *Int. J. Infect. Dis.* **51**, 135-138.

Zhang, F., Hammack, C., Ogden, S. C., Cheng, Y., Lee, E. M., Wen, Z., Qian, X., Nguyen, H. N., Li, Y., Yao, B. et al. (2016). Molecular signatures associated with ZIKV exposure in human cortical neural progenitors. *Nucleic Acids Res.* **44**, 8610-8620.